



Communication

Electrically Polarized Graphene-Blended Spacers for Organic Fouling Reduction in Forward Osmosis

Numan Yanar ¹, Yejin Liang ¹, Eunmok Yang ¹, Hosik Park ^{2,*}, Moon Son ^{3,*} and Heechul Choi ^{1,*}

- ¹ School of Earth Sciences and Environmental Engineering, Gwangju Institute of Science and Technology (GIST), 123-Cheomdangwagi-ro, Buk-gu, Gwangju 61005, Korea; numanyanar@gm.gist.ac.kr (N.Y.); liangyejin@gist.ac.kr (Y.L.); yang1990@gist.ac.kr (E.Y.)
- ² Green Carbon Research Center, Chemical Process Division, Korea Research Institute of Chemical Technology (KRICT), Daejeon 34114, Korea
- ³ School of Urban and Environmental Engineering, Ulsan National Institute of Science and Technology, 50, UNIST-gil, Eonyang-eup, Ulju-gun, Ulsan 44919, Korea
- * Correspondence: hspark@kRICT.re.kr (H.P.); moonson619@unist.ac.kr (M.S.); hcchoi@gist.ac.kr (H.C.); Tel.: +82-62-715-2441 (H.C.); Fax: +82-62-715-2423 (H.C.)

Abstract: In membrane processes, a spacer is known to play a key role in the mitigation of membrane fouling. In this study, the effect of electric polarization on a graphene-blended polymer spacer (e.g., poly(lactic acid), PLA) for organic fouling on membrane surfaces was investigated. A pristine PLA spacer (P-S), a graphene-blended spacer (G-S), and an electrically polarized graphene-blended spacer (EG-S) were successfully fabricated by 3D printing. Organic fouling tests were conducted by the 5-h filtration of CaCl₂ and a sodium alginate solution through commercially available membranes, which were placed together with the fabricated spacers. Membranes utilizing P-S, G-S, and EG-S were characterized in terms of the fouling amount on the membrane surface and fouling roughness. Electrostatic forces of EG-S provided 70% less and 90% smoother fouling on the membrane surface, leading to an only 14% less water flux reduction after 5 h of fouling. The importance of nanomaterial blending and polarization was successfully demonstrated herein.

Keywords: organic fouling; electrically polarized spacer; 3D printed spacer; forward osmosis; graphene-blended spacers; nanomaterial-blended spacers



Citation: Yanar, N.; Liang, Y.; Yang, E.; Park, H.; Son, M.; Choi, H. Electrically Polarized Graphene-Blended Spacers for Organic Fouling Reduction in Forward Osmosis. *Membranes* **2021**, *11*, 36. <https://doi.org/10.3390/membranes11010036>

Received: 14 December 2020

Accepted: 29 December 2020

Published: 4 January 2021

Publisher's Note: MDPI stays neutral with regard to jurisdictional claims in published maps and institutional affiliations.



Copyright: © 2021 by the authors. Licensee MDPI, Basel, Switzerland. This article is an open access article distributed under the terms and conditions of the Creative Commons Attribution (CC BY) license (<https://creativecommons.org/licenses/by/4.0/>).

1. Introduction

Membrane treatment methods have been playing a crucial role in providing potable water [1]. As a result of the depletion of fresh water sources due to global warming [2], these methods are gaining increasing importance. However, energy efficiency, which is directly related to membrane permselectivity, must be maintained well even after long-term use [3,4]. Fouling, concentration polarization, and mechanical damage of the membranes are the most critical factors that directly affect the membrane performance and energy efficiency [5–8]. Among these factors, membrane fouling in membrane systems is the most crucial issue that needs to be considered, especially because brackish water, wastewater and seawater comprise a number of foulants that can block the membrane surface and pores, thereby reducing the productivity of treated water [5,9].

Various types of membrane fouling include crystalline fouling, organic fouling, particle fouling, colloidal fouling, and biofouling [10,11]. Among these types, organic fouling serves as the major constraint due to the presence of relatively high concentrations of organics in water [12]. Organic fouling is a critical issue for all types of filtration membranes, including microfiltration (MF), ultrafiltration (UF), nanofiltration (NF), reverse osmosis (RO), and forward osmosis (FO). Organic fouling results from the aggregation of organic materials such as proteins, sugar, humic-acid-like substances and polysaccharides on the membrane surface [13,14]. Proteins creating organic fouling are present in a high

ratio in wastewater, which aggregate on the membrane surface due to hydrogen bonding between the molecules [13]. This aggregation leads to severe fouling, which in turn decreases the performance, i.e., water production capacity.

FO membranes demonstrate immense potential and extensive applications to reduce the total energy consumption during desalination and waste water treatment. As a result of benefitting from the draw solution with a high osmotic concentration, FO systems can filter water with foulants without the use of any external pressure through high-pressure pumps [15]. As FO is responsible for handling water contaminants rather than desalting, organic fouling is highly critical for this system. Previously, Zhao et al. reported that organic fouling is more severe and irreversible in FO systems [16]. FO fouling results from effects of chemical and hydrodynamic interactions. A fouling layer is developed on the membrane surface by major factors, including calcium binding, permeation drag, and hydrodynamic shear force [17]. In this regard, approaches including the use of fouling-resistant novel membranes, change in the hydrodynamic conditions, use of membrane feed spacers, and pre/post-treatment are mainly employed to mitigate organic fouling. Among these approaches, feed spacers have been extensively investigated thus far as spacers for an FO membrane module are essential for maintaining a flow channel and providing hydrodynamic conditions [18]. An effective feed spacer also should work well for reducing foulant deposition and concentration polarization [19].

Various studies on feed spacers have focused on the spacer shape [19,20]. Previous studies employed computational fluid dynamics (CFD) to investigate the effect of spacer shapes, including nonwoven, woven, middle layer, and fully woven spacers [21]; 30°, 45°, 62°, and 90° spacer filaments [22]; hairy spacers [23]; saw-tooth spacers [24]; zigzag spacers [25]; multi-layer spacers [26]; and sinusoidal spacers [27], on the membrane performance. In addition, with the boost of 3D printing, the design of spacers was affected [28,29], i.e., column-type spacers [30], triply periodic minimal surfaces (TPMS) spacers [31], symmetric perforated spacers (1-Hole, 2-Hole, and 3-Hole) [32], and honeycomb spacers [33], were fabricated by 3D printing. In addition, 3D printing provides material selection for spacer fabrication. Previously, our group investigated the performance of 3D printed spacers comprising acrylonitrile-butadiene-styrene, (poly(lactic acid), PLA), and polypropylene. Spacers composed of different materials exhibit different performances [34]. Benefitting from recent developments in 3D printing, our group also recently introduced a graphene-blended membrane spacer and investigated the effect of electric polarization on the graphene-blended spacer [35]. Through that work, we reported the performance of the electrically polarized graphene-blended spacer as a draw spacer for flux enhancement, and as a feed spacer for membrane scaling. Apart from scaling, organic fouling is also a critical issue that has to be addressed due to its sticky nature. By considering the importance of mitigating organic fouling of FO membranes, the electrically polarized graphene spacer was further investigated in this study. To the best of our knowledge, this is the first study of an electrically polarized graphene-blended polymer spacer for the mitigation of organic fouling.

2. Materials and Methods

Three fabricated spacers prepared by 3D printing after computer-aided design (CAD) modelling were used for experiments. One PLA and two graphene-blended PLA spacers were fabricated by using the same structural parameters (i.e., spacer filament thickness of 1.27 mm, with a vertical and horizontal spacer hole distance of 7 mm) (Figure 1). All spacers were fabricated by using a fused deposition modelling (FDM)-type 3D printer (OpenCreators-Almond, Gyeonggi, Korea). PLA spacer was fabricated by using a PLA filament (PLABS, Gyeonggi, Korea) which has 1.24 gm/cm³ specific gravity, 26.4 MPa tensile strength, 2.3 GPa tensile modulus and elongation break at 4%, and graphene-blended PLA spacers were fabricated by using conductive graphene blended PLA filaments which has 1.11 gm/cm³ specific gravity, 53 MPa tensile strength, 2.9 GPa tensile modulus and elongation break at 5.1% (Graphene Laboratories, Ronkonkoma, NY, USA) [36]. Later,

one of the graphene-blended PLA spacers was electrically polarized under an electric field of 1.5 kV/cm for 2 h. Further details regarding the fabrication of the spacers by using FDM type 3D printer as well as electric polarization were reported in another article by our group [35]. In this article, PLA, graphene-blended poly(lactic acid), and electrically polarized graphene-blended PLA spacers were denoted as P-S, G-S, and EG, respectively.

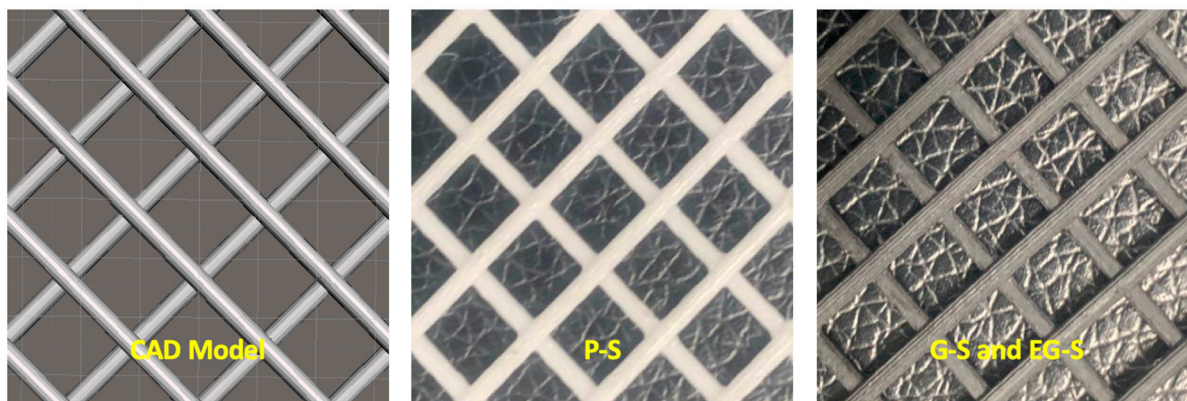


Figure 1. CAD model; 3D printed poly(lactic acid) (P-S); graphene-blended poly(lactic acid) (G-S); and electrically polarized graphene-blended poly(lactic acid) (EG-S).

Flux measurements were conducted for pure water flux/reverse solute flux measurements and fouling-based flux reduction. For the performance investigation of the spacers, commercial membranes (Porifera, San Leandro, CA, USA) were used, which were extracted from a commercial membrane module. An engineered osmosis system (Figure S1) with an effective filtration area of 19.35 cm² was utilized in the continuous filtration mode at a cross flow rate of 200 cm³/s for the draw and feed sides (Figure 2). For the pure water flux and reverse solute flux measurements, a 0.6 M NaCl (Sigma-Aldrich, Burlington, MA, USA) solution was prepared as the draw solution, and deionized (DI) water (Synergy, Millipore, Billerica, MA, USA) with a resistivity of 18.2 mΩ-cm at 25 °C was used as the feed solution. Filtration was conducted for 1 h for each sample, with 5 times repetition. For the fouling experiment, an alginate-based feed solution was prepared, while 0.6 M NaCl was used as the draw solution. As the fouling solution, 200 ppm of C₆H₉NaO₇ (sodium alginate, Sigma-Aldrich, Burlington, MA, USA) and 1 mM of CaCl₂ (Sigma-Aldrich, Burlington, MA, USA) were dissolved in DI water [37]. Here, CaCl₂ was used as the Ca²⁺ source to bind alginate molecules. Filtration was conducted for 5 h after flux stabilization was performed for 1 h. Data obtained by the weight change in the feed solution in pure flux and fouling experiments, as well as feed conductivity for only pure flux experiments, were recorded every minute by a connected computer. From these recorded values, the water flux, J_w , and the reverse solute flux, J_s , were calculated by using the following formulas [38,39]:

$$J_w = \frac{V}{A_m \Delta t} \quad (1)$$

$$J_s = \frac{V_t C_t - V_0 C_0}{A_m t} \quad (2)$$

In the first formula, J_w is the water flux, V is the volume of permeated water (L), A_m is the effective membrane area (m²), and Δt is the permeation time (min). The reverse solute flux was calculated from the electrical feed conductivity per minute [39]. In the second formula, C_t is the concentration (g/L) at time t , V_t is the volume (L) of the feed solution at time t , C_0 is the initial concentration (g/L), and V_0 the initial volume (L) of the feed solution. The resulting values were converted into Lm⁻²h⁻¹ (LMH) for water flux and gm⁻²h⁻¹ (gMH) for reverse solute flux.

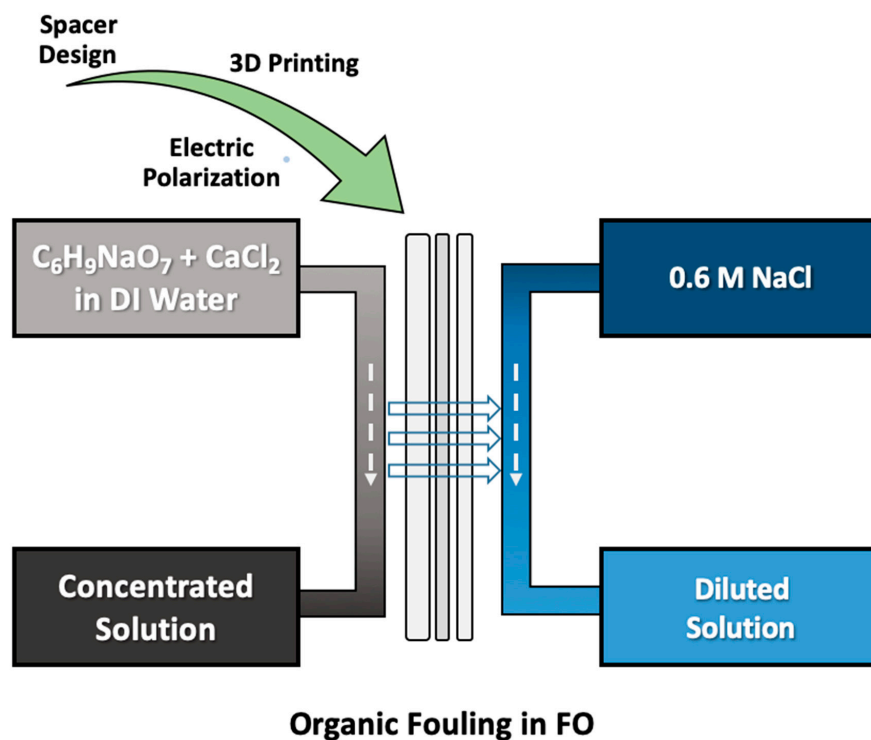


Figure 2. Organic fouling test of 3D printed spacers through a forward osmosis system.

Surface roughness of fouled membranes, foulant volume on membranes, and visual topographic images of fouled membranes were obtained by a Surface Nano-Profiler (Nanomap-D/Alpha-steps, HTSK, Gyeonggi, Korea) measurements. 3D measurements were performed with an x–y scanning distance of 500 μm and a scanning speed of 50 $\mu\text{m}/\text{s}$ at 10 steps for each sample. These measurements were repeated 10 times for each sample. Notably, characterization was performed for surface areas that were not in contact with the spacers.

The amounts of foulant adsorbed on the G-S and EG-S spacers were investigated by dipping the spacers in 200 mL of an alginate solution for 12 h (same solution as mentioned above) at room temperature. Spacer weights were measured before and after the dipping process (after drying in an oven at 40 $^{\circ}\text{C}$ for 2 h). Later, spacers were cleaned in an ultrasonicator (B8510-MT, Branson, Brookfield, CT, USA) by dipping in DI water. After cleaning in an oven at 40 $^{\circ}\text{C}$ for 2 h, the spacer weight was measured again. Finally, the amounts of foulant adsorbed on G-S and EG-S spacers (before and after cleaning) were obtained. Notably, the resistance of spacers against heating and sonication was repetitively tested by using non-fouled spacers. G-S and EG-S spacers did not exhibit any deformation, while the P-S spacer exhibited weight loss and structural deformation. Therefore, the P-S spacer is not included in this investigation.

3. Results and Discussion

P-S and two G-S spacers were successfully printed, and one of the G-S spacers was polarized to obtain an electrically polarized EG-S spacer. All three samples were examined for pure water flux and reverse solute flux measurements. Flux performances of all three spacers were relatively similar. More specifically, P-S, G-S, and EG-S exhibited water flux of 13 ± 0.85 LMH, 12.8 ± 0.55 , and 14.4 ± 0.69 LMH, respectively (Figure 3). In addition, similar values for reverse solute fluxes were observed: 7.2 ± 1.8 gMH for P-S, 8.1 ± 1 gMH for G-S, and 7.3 ± 2.2 gMH for EG-S (Figure 3). Marginal changes in the flux values were attributed to the same structure of spacers.

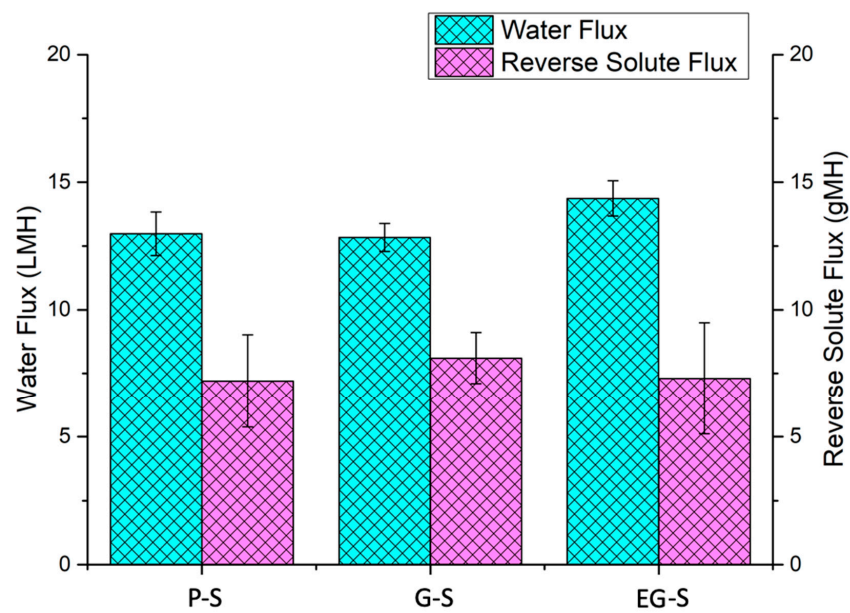


Figure 3. Water fluxes and reverse solute fluxes for P-S, G-S, and EG-S spacers.

Additional tests were performed to investigate the organic fouling performance of P-S, G-S, and EG-S spacers. After 5 h of alginate-based fouling of membrane spacers, the fouled membranes with P-S or G-S exhibited a water flux reduction of 31% or 33%, respectively (Figure 4). This ratio was found to be 14% of the water flux for the fouled membranes with the EG-S spacer. Even though graphene blending did not considerably affect the performance of the PLA spacer for water flux reduction, the electric polarization of the graphene-blended spacer was highly effective in preventing the water flux reduction of the EG-S membrane.

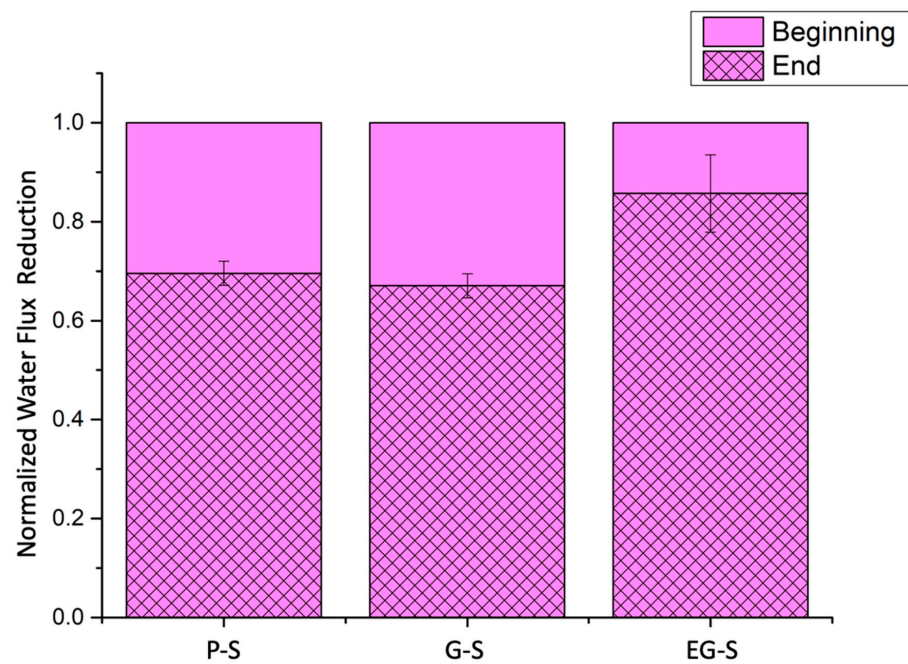


Figure 4. Normalized water flux reduction for the P-S, G-S, and EG-S membranes.

To understand the fouling phenomena, fouling characterization of the P-S, G-S, and EG-S fouled membranes was further performed using the Surface Nano-profiler via the analysis of the foulant volume and roughness, and representative images were

obtained. The Surface Nano-profiler permitted the characterization of fouling in a larger area compared to other topographic fouling characterization methods. Results obtained from the surface nano-profiler also supported the data obtained from water flux reduction. On a $500 \times 500 \mu\text{m}^2$ area, P-S, G-S, and EG-S membranes exhibited $12,685 \pm 759 \mu\text{m}^3$, $12,391 \pm 848 \mu\text{m}^3$, and $3570 \pm 824 \mu\text{m}^3$ foulant, respectively, from an average of 10 measurements for each membrane (Figure 5). The membrane with the EG-S spacer exhibited 70% less foulant on its surface. The presence of Ca^{2+} in the fouling solution induces bridges between the negatively charged alginate molecules [40,41], resulting in positively charged Ca-alginate bridges [42,43]. That is, positive Ca^{2+} binds to negatively charged carboxylic groups of alginate [44], which is defined as the egg-box model in literature to explain the interaction between polysaccharides and divalent cations [45]. This generates aggregation as well as a compact fouling layer on the membrane surface [46]. Hence, roughness of fouled membranes is observed. Roughness (Ra) values of $1.25 \mu\text{m}$, $1.28 \mu\text{m}$, and $0.12 \mu\text{m}$ were obtained for the P-S, G-S, and EG-S fouled membranes, respectively. In addition, the smooth fouled surface of EG-S as well as rough fouled surfaces of P-S and G-S were observed in the representative characterization images from the surface nano-profiler (Figure 6). Here, the surfaces can be explained by the manipulation of a positively charged Ca-alginate bridge and physically bonded Ca^{2+} by the EG-S electrostatic forces. In a previous study reported by our group, the polarized spacer was found to exhibit dominating negative charges [35]. Therefore, positively charged Ca-alginate bridges are readily deposited on the negatively charged spacers. Furthermore, EG-S reduces the physical binding effect of Ca^{2+} between alginate molecules, and the aggregation of alginate molecules is less on the membrane surface, which can be understood from the lower roughness value of the EG-S membrane. Hence, fouling on the EG-S membrane is less than that on the P-S and G-S membranes.

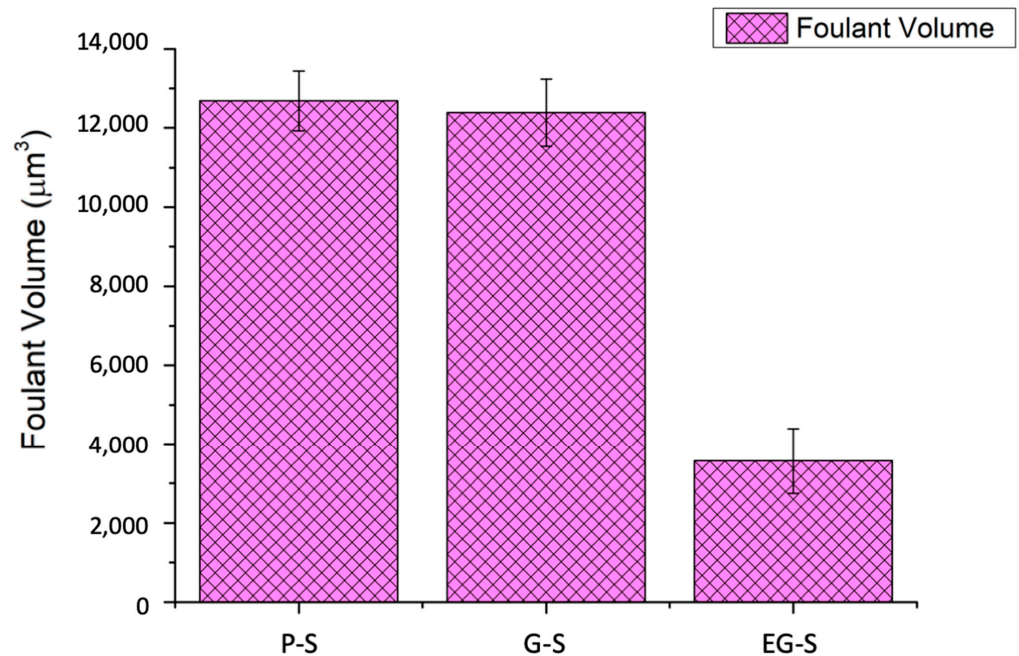


Figure 5. Average foulant volume for the fouled membranes with the P-S, G-S, and EG-S spacers.

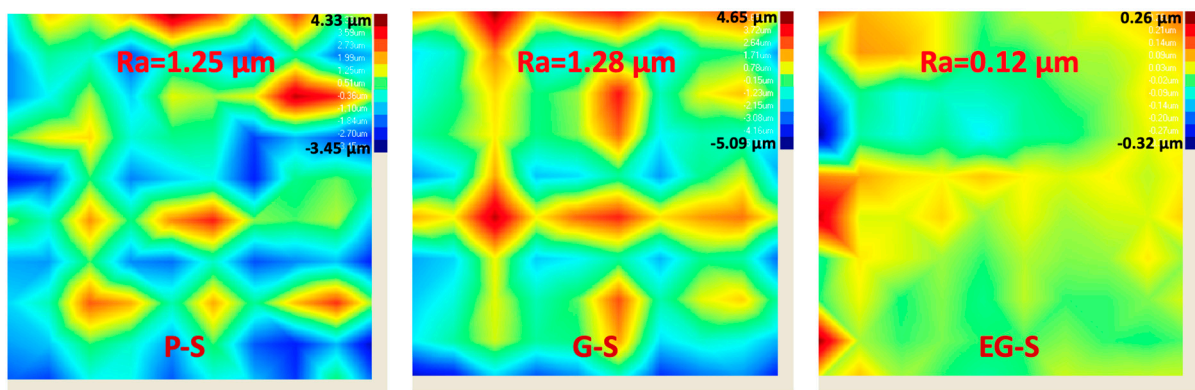


Figure 6. Surface profiles of the P-S, G-S, and EG-S fouled membranes (Roughness values also are provided on each figure). (Blue and red colors represent low fouling and high fouling thicknesses, respectively).

By considering the spacer fouling issue, the effect of electric polarization was further investigated by measuring the total adsorbed foulant amount on the spacers G-S and EG-S. After dipping the G-S and EG-S spacers for 12 h, 20 mg and 31 mg foulants were adsorbed, respectively. After the cleaning process, both spacers exhibited the same amount of foulant on the surface (20 mg) (Figure 7). In here, electric polarization permitted the deposition of the foulant on EG-S with weaker adhesion, leading to a lower foulant deposition on the EG-S membrane.

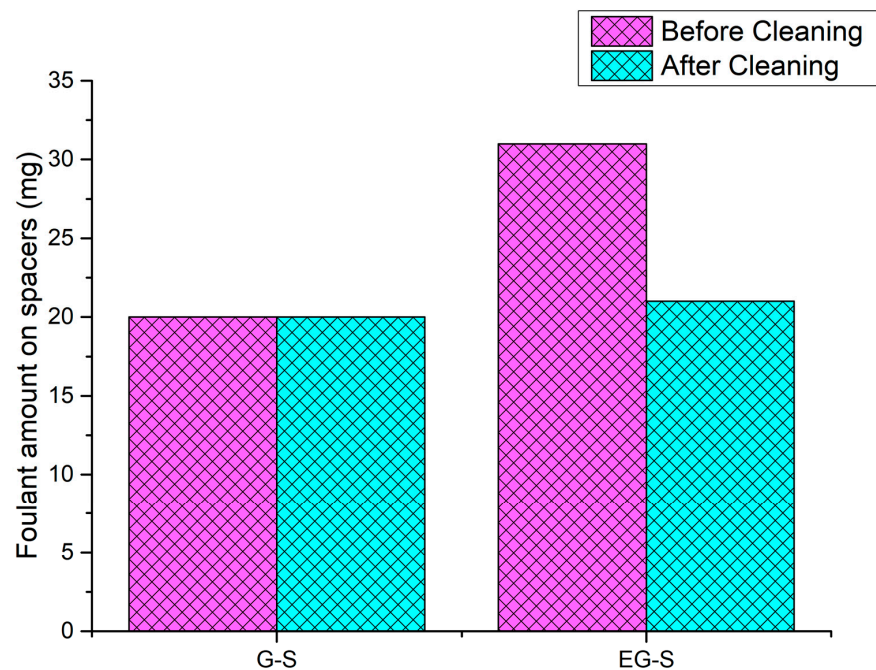


Figure 7. Efficacy of electric polarization on the adsorption of foulants on the G-S and EG-S spacers.

4. Conclusions

In this article, the performance of electrically polarized graphene-blended poly(lactic acid) spacer (EG-S) was analyzed for alginate fouling. Compared to P-S and G-S, EG-S exhibited 70% less fouling on the membrane surface with a smoother fouling layer. Therefore, only 14% water flux reduction ratio was observed for the membrane of EG-S, while it was 31% or 33% for the membranes of P-S or G-S, respectively. This EG-S performance was attributed to the electrostatic manipulation of Ca-alginate bridges and Ca^{2+} ions which are binding alginate molecules. Regarding to this, foulant adsorption test G-S and EG-S also showed that EG-S can collect 55% more foulant on itself than G-S, and it was also

investigated that this additional amount of foulant collected by the effect of electric polarization is cleanable. However, this point should be extensively studied further in another research. For future studies, high-pressure membrane systems such as NF or RO also should be considered by utilizing various organic foulants such as humic acid or bovine serum albumin.

Supplementary Materials: The following are available online at <https://www.mdpi.com/2077-0375/11/1/36/s1>, Figure S1: Engineered osmosis system.

Author Contributions: Conceptualization, N.Y.; methodology, N.Y., Y.L. and E.Y.; software, N.Y.; validation, N.Y., M.S., H.P. and H.C.; formal analysis, N.Y. and M.S.; investigation, N.Y. and M.S.; resources, N.Y. and H.C.; data curation, N.Y., M.S., H.P. and H.C.; writing—original draft preparation, N.Y.; writing—review and editing, N.Y., M.S., H.P., Y.L., E.Y. and H.C.; visualization, N.Y.; supervision, H.C., M.S. and H.P.; project administration, H.C.; funding acquisition, H.C. All authors have read and agreed to the published version of the manuscript.

Funding: This study was supported by National Research Foundation of Korea (NRF) projects funded by Korean Government (MSIT) with grant numbers of No. 2020R1A2C2010808 and No. 2020M3H5A1081105.

Institutional Review Board Statement: Not applicable.

Informed Consent Statement: Not applicable.

Data Availability Statement: Not applicable.

Conflicts of Interest: The authors declare no conflict of interest.

References

1. Ciardelli, G.; Corsi, L.; Marcucci, M. Membrane separation for wastewater reuse in the textile industry. *Resour. Conserv. Recycl.* **2001**, *31*, 189–197.
2. Yanar, N.; Choi, H. Urban Water Management and Quality-Based Water Use. *Iglus Q.* **2019**, *5*, 4–6.
3. Rezakazemi, M.; Dashti, A.; Harami, H.R.; Hajilari, N. Fouling-resistant membranes for water reuse. *Environ. Chem. Lett.* **2018**, *16*, 715–763.
4. Panchal, C.B.; Knudsen, J.G. Mitigation of water fouling: Technology status and challenges. *Adv. Heat Transf.* **1998**, *31*, 431–474.
5. She, Q.; Wang, R.; Fane, A.G.; Tang, C.Y. Membrane fouling in osmotically driven membrane processes: A review. *J. Membr. Sci.* **2016**, *499*, 201–233.
6. Persson, K.M.; Gekas, V.; Trägårdh, G. Study of membrane compaction and its influence on ultrafiltration water permeability. *J. Membr. Sci.* **1995**, *100*, 155–162.
7. Lin, S.; Buehler, M.J. Mechanics and molecular filtration performance of graphyne nanoweb membranes for selective water purification. *Nanoscale* **2013**, *5*, 11801–11807.
8. Hoek, E.M.V.; Elimelech, M. Cake-enhanced concentration polarization: A new fouling mechanism for salt-rejecting membranes. *Environ. Sci. Technol.* **2003**, *37*, 5581–5588.
9. Kimura, K.; Hane, Y.; Watanabe, Y.; Amy, G.; Ohkuma, N. Irreversible membrane fouling during ultrafiltration of surface water. *Water Res.* **2004**, *38*, 3431–3441.
10. Flemming, H.C.; Schaule, G.; McDonogh, R. Biofouling on Membranes—A Short Review. In *Biofilms—Science and Technology*; Melo, L.F., Bott, T.R., Fletcher, M., Capdeville, B., Eds.; Springer: Dordrecht, The Netherlands, 1992; pp. 487–497. [[CrossRef](#)]
11. Celik Madenli, E.; Yanar, N.; Choi, H. Enhanced antibacterial properties and suppressed biofilm growth on multi-walled carbon nanotube (MWCNT) blended polyethersulfone (PES) membranes. *J. Environ. Chem. Eng.* **2020**. [[CrossRef](#)]
12. Amy, G. Fundamental understanding of organic matter fouling of membranes. *Desalination* **2008**, *231*, 44–51. [[CrossRef](#)]
13. Aftab, B.; Ok, Y.S.; Cho, J.; Hur, J. Targeted removal of organic foulants in landfill leachate in forward osmosis system integrated with biochar/activated carbon treatment. *Water Res.* **2019**, *160*, 217–227. [[CrossRef](#)]
14. Yadav, S.; Ibrar, I.; Bakly, S.; Khanafer, D.; Altaee, A.; Padmanaban, V.C.; Samal, A.K.; Hawari, A.H. Organic Fouling in Forward Osmosis: A Comprehensive Review. *Water* **2020**, *12*, 1505. [[CrossRef](#)]
15. Parida, V.; Ng, H.Y. Forward osmosis organic fouling: Effects of organic loading, calcium and membrane orientation. *Desalination* **2013**, *312*, 88–98. [[CrossRef](#)]
16. Zhao, S.; Zou, L.; Mulcahy, D. Effects of membrane orientation on process performance in forward osmosis applications. *J. Membr. Sci.* **2011**, *382*, 308–315. [[CrossRef](#)]
17. Mi, B.; Elimelech, M. Chemical and physical aspects of organic fouling of forward osmosis membranes. *J. Membr. Sci.* **2008**, *320*, 292–302. [[CrossRef](#)]
18. Xie, M.; Tang, C.Y.; Gray, S.R. Spacer-induced forward osmosis membrane integrity loss during gypsum scaling. *Desalination* **2016**, *392*, 85–90. [[CrossRef](#)]

19. Abid, H.S.; Johnson, D.J.; Hashaikeh, R.; Hilal, N. A review of efforts to reduce membrane fouling by control of feed spacer characteristics. *Desalination* **2017**, *420*, 384–402. [[CrossRef](#)]
20. Koo, J.W.; Ho, J.S.; An, J.; Zhang, Y.; Chua, C.K.; Chong, T.H. A review on spacers and membranes: Conventional or hybrid additive manufacturing? *Water Res.* **2021**, *188*, 116497. [[CrossRef](#)]
21. Gu, B.; Adjiman, C.S.; Xu, X.Y. The effect of feed spacer geometry on membrane performance and concentration polarisation based on 3D CFD simulations. *J. Membr. Sci.* **2017**, *527*, 78–91. [[CrossRef](#)]
22. Taamneh, Y.; Bataineh, K. Improving the performance of direct contact membrane distillation utilizing spacer-filled channel. *Desalination* **2017**, *408*, 25–35. [[CrossRef](#)]
23. Li, W.; Chen, K.K.; Wang, Y.-N.; Krantz, W.B.; Fane, A.G.; Tang, C.Y. A conceptual design of spacers with hairy structures for membrane processes. *J. Membr. Sci.* **2016**, *510*, 314–325. [[CrossRef](#)]
24. Liu, J.; Liu, Z.; Xu, X.; Liu, F. Saw-tooth spacer for membrane filtration: Hydrodynamic investigation by PIV and filtration experiment validation. *Chem. Eng. Process. Process Intensif.* **2015**, *91*, 23–34. [[CrossRef](#)]
25. Schwinge, J.; Wiley, D.E.; Fane, A.G.; Guenther, R. Characterization of a zigzag spacer for ultrafiltration. *J. Membr. Sci.* **2000**, *172*, 19–31. [[CrossRef](#)]
26. Balster, J.; Pünt, I.; Stamatiadis, D.F.; Wessling, M. Multi-layer spacer geometries with improved mass transport. *J. Membr. Sci.* **2006**, *282*, 351–361. [[CrossRef](#)]
27. Xie, P.; Murdoch, L.C.; Ladner, D.A. Hydrodynamics of sinusoidal spacers for improved reverse osmosis performance. *J. Membr. Sci.* **2014**, *453*, 92–99. [[CrossRef](#)]
28. Yanar, N.; Kallem, P.; Son, M.; Park, H.; Kang, S.; Choi, H. A New era of water treatment technologies: 3D printing for membranes. *J. Ind. Eng. Chem.* **2020**. [[CrossRef](#)]
29. Yanar, N.; Son, M.; Park, H.; Choi, H. Toward greener membranes with 3D printing technology. *Environ. Eng. Res.* **2020**, *26*, 200027. [[CrossRef](#)]
30. Ali, S.M.; Qamar, A.; Kerdi, S.; Phuntsho, S.; Vrouwenvelder, J.S.; Ghaffour, N.; Shon, H.K. Energy efficient 3D printed column type feed spacer for membrane filtration. *Water Res.* **2019**, *164*, 114961. [[CrossRef](#)]
31. Sreedhar, N.; Thomas, N.; Al-Ketan, O.; Rowshan, R.; Hernandez, H.; Al-Rub, R.K.A.; Arafat, H.A. 3D printed feed spacers based on triply periodic minimal surfaces for flux enhancement and biofouling mitigation in RO and UF. *Desalination* **2018**, *425*, 12–21. [[CrossRef](#)]
32. Kerdi, S.; Qamar, A.; Vrouwenvelder, J.S.; Ghaffour, N. Fouling resilient perforated feed spacers for membrane filtration. *Water Res.* **2018**, *140*, 211–219. [[CrossRef](#)] [[PubMed](#)]
33. Yanar, N.; Son, M.; Park, H.; Choi, H. Bio-mimetically inspired 3D-printed honeycombed support (spacer) for the reduction of reverse solute flux and fouling of osmotic energy driven membranes. *J. Ind. Eng. Chem.* **2020**, *83*, 343–350. [[CrossRef](#)]
34. Yanar, N.; Son, M.; Yang, E.; Kim, Y.; Park, H.; Nam, S.-E.; Choi, H. Investigation of the performance behavior of a forward osmosis membrane system using various feed spacer materials fabricated by 3D printing technique. *Chemosphere* **2018**, *202*, 708–715. [[CrossRef](#)] [[PubMed](#)]
35. Yanar, N.; Park, H.; Son, M.; Choi, H. Efficacy of Electrically-Polarized 3D Printed Graphene-blended Spacers on the Flux Enhancement and Scaling Resistance of Water Filtration Membranes. *arXiv* **2020**, arXiv:2012.07210.
36. Camargo, J.C.; Machado, Á.R.; Almeida, E.C.; Silva, E.F.M.S. Mechanical properties of PLA-graphene filament for FDM 3D printing. *Int. J. Adv. Manuf. Technol.* **2019**, *103*, 2423–2443. [[CrossRef](#)]
37. Salehi, H.; Rastgar, M.; Shakeri, A. Anti-fouling and high water permeable forward osmosis membrane fabricated via layer by layer assembly of chitosan/graphene oxide. *Appl. Surf. Sci.* **2017**, *413*, 99–108. [[CrossRef](#)]
38. Nguyen, H.T.; Nguyen, N.C.; Chen, S.-S.; Li, C.-W.; Hsu, H.-T.; Wu, S.-Y. Innovation in Draw Solute for Practical Zero Salt Reverse in Forward Osmosis Desalination. *Ind. Eng. Chem. Res.* **2015**, *54*, 6067–6074. [[CrossRef](#)]
39. Son, M.; Choi, H.; Liu, L.; Park, H.; Choi, H. Optimized Synthesis Conditions of Polyethersulfone Support Layer for Enhanced Water Flux for Thin Film Composite Membrane. *Environ. Eng. Res.* **2014**, *19*, 339–344. [[CrossRef](#)]
40. Van den Brink, P.; Zwijnenburg, A.; Smith, G.; Temmink, H.; van Loosdrecht, M. Effect of free calcium concentration and ionic strength on alginate fouling in cross-flow membrane filtration. *J. Membr. Sci.* **2009**, *345*, 207–216. [[CrossRef](#)]
41. Son, M.; Choi, H.-g.; Liu, L.; Celik, E.; Park, H.; Choi, H. Efficacy of carbon nanotube positioning in the polyethersulfone support layer on the performance of thin-film composite membrane for desalination. *Chem. Eng. J.* **2015**, *266*, 376–384. [[CrossRef](#)]
42. Clogston, J.D.; Patri, A.K. Zeta Potential Measurement. In *Characterization of Nanoparticles Intended for Drug Delivery*; McNeil, S.E., Ed.; Humana Press: Totowa, NJ, USA, 2011; pp. 63–70. [[CrossRef](#)]
43. Szekalska, M.; Sosnowska, K.; Czajkowska-Kośnik, A.; Winnicka, K. Calcium chloride modified alginate microparticles formulated by the spray drying process: A strategy to prolong the release of freely soluble drugs. *Materials* **2018**, *11*, 1522. [[CrossRef](#)] [[PubMed](#)]
44. Lee, S.; Elimelech, M. Relating Organic Fouling of Reverse Osmosis Membranes to Intermolecular Adhesion Forces. *Environ. Sci. Technol.* **2006**, *40*, 980–987. [[CrossRef](#)] [[PubMed](#)]
45. Grant, G.T.; Morris, E.R.; Rees, D.A.; Smith, P.J.C.; Thom, D. Biological interactions between polysaccharides and divalent cations: The egg-box model. *Febs Lett.* **1973**, *32*, 195–198. [[CrossRef](#)]
46. Ye, W.; Bernstein, N.J.; Lin, J.; Jordens, J.; Zhao, S.; Tang, C.Y.; van der Bruggen, B. Theoretical and experimental study of organic fouling of loose nanofiltration membrane. *J. Taiwan Inst. Chem. Eng.* **2018**, *93*, 509–518. [[CrossRef](#)]